Journal of Geriatric Cardiology | JGC
RESEARCH ARTICLE
J Geriatr Cardiol 2024; 21(12): 1119–1132

The effects of hypothalamic microglial activation on ventricular arrhythmias in stress cardiomyopathy

Peng-Qi LIN[1,*], Quan-Wei PEI[1,*], Bin LI[1,*], Jie-Mei YANG[2], Li-Na ZOU[1], De-Zhan SU[1], Jun-Pei ZHANG[1], Hong-Peng YIN[1], Mbabazi Nadine[1], Jun-Jie YANG[1], Nevzorova Vera A[3], Khan Musawir Abbas[1], Zhao-Lei JIANG[4,✉], Jing-Jie LI[1,✉], De-Chun YIN[5,✉]

1. Department of Cardiology, the First Affiliated Hospital of Harbin Medical University, Harbin, China; 2. Department of Echocardiography, the First Affiliated Hospital of Harbin Medical University, Harbin, China; 3. Institute Therapy and Instrumental Diagnostic, Pacific State Medical University, Vladivostok, Russia; 4. Department of Cardiothoracic Surgery, Xinhua Hospital, School of Medicine, Shanghai Jiaotong University, Shanghai, China; 5. Department of Geriatrics, the First Affiliated Hospital of Harbin Medical University, Harbin, China

*The authors contributed equally to this manuscript

✉ Correspondence to: yindechun@hrbmu.edu.cn (YIN DC); wojiangzhaolei@163.com (JIANG ZL); lijingjie@hrbmu.edu.cn (LI JJ)

https://doi.org/10.26599/1671-5411.2024.12.002

ABSTRACT

Background Stress cardiomyopathy (SCM) currently has a high incidence in older adults, and the theories regarding its causes include "catecholamine myocardial toxicity" and "sympathetic hyperactivation". However, the role of the central nervous system in the pathogenesis of SCM remains unknown. We investigated the role of microglia activation in the paraventricular hypothalamic nucleus (PVN) in the development of SCM.

Methods An SCM model was created using male Sprague-Dawley (SD) rats, immobilized for 6 h every day for a week. Electrocardiogram, cardiac electrophysiology, and echocardiography examinations were performed to verify the changes in cardiac structure and function in rats with SCM. RNA sequencing was used to explore the changes in the hypothalamus during SCM. In addition, brain and heart tissues were collected to detect microglial activation and sympathetic activity.

Results The main findings were as follows: (1) immobilization stress successfully induced SCM in SD rats; (2) microglia were significantly activated in the hypothalamus, as evidenced by cytosol thickening, increases in the number of microglial branches, and microglia enriched in the PVN; (3) in SCM, the microglia in the PVN exhibited increased central and peripheral cardiac sympathetic activity and increased the expression of neuroinflammatory factors; and (4) it is possible that inhibiting microglial activation could suppress the sympathetic activity of the central nervous system and heart and increase cardiac electrical stability in SCM rats.

Conclusions SCM was induced in SD rats by immobilization stress, acting through the activation of the hypothalamic microglia. The activated microglia were specifically enriched in the PVN, increasing the activity of the central and peripheral sympathetic nervous systems by regulating the expression of neuro-inflammatory factors, mediating dysfunction of the left ventricle, and increasing the susceptibility to ventricular arrhythmias.

Stress cardiomyopathy (SCM) is a reversible and transient abnormality of the left ventricular systolic and diastolic functions, similar to myocardial infarction but in the absence of coronary artery disease. SCM, also referred to as Tako-Tsubo cardiomyopathy, was first described in Japan in the 1990s and is characterized by transient left ventricular dysfunction.[1–4] SCM has an incidence of 1.0%-2.5%, with the majority of cases occurring in postmenopausal women, frequently in response to acute emotional or physical stress.[2] While the frequency of SCM has been growing (15–30 cases per 100,000 people per year), its true rate of occurrence is unclear due to under-diagnosis.[5] The in-hospital mortality rate is 1.0%–4.5%, and there is a recurrence rate of 5%–10% among SCM patients after a 5-year follow-up.[6] SCM has a high incidence in older adults. Of 112 patients enrolled in the Chinese Registry of Takotsubo Syndrome from 02/01/2016 to 12/28/2021, the mean age was 59.4 ± 18.7 years, and 27.7% were men.[7] Patients with SCM are more prone to life-threatening ventricular

arrhythmias such as ventricular tachycardia, ventricular fibrillation (VF), tip-twist, and sudden cardiac death.[8] SCM is associated with sympathetic hyperactivity, catecholamine myocardial toxicity, abnormalities in microvascular and myocardial metabolism, coronary vasospasm,[5,9] elevated levels of plasma catecholamines and their metabolites, inflammation, and estrogen deficiency.[1] However, the exact pathophysiological mechanisms in the central nervous system (CNS) involved with SCM remain unclear.[10]

Although a connection between the brain and the heart has long been proposed, the role of the CNS in the pathogenesis of SCM is still uncertain. The CNS contains numerous glial cells,[11] which have been found to play an important role in regulating neuronal development, maintaining homeostasis in the brain and the blood-brain barrier,[12] and modulating neuronal activity.[13] Microglia are a type of glial cell and release neuroactive molecules called gliotransmitters, including pro-inflammatory cytokines, chemokines, proteases, reactive oxygen/nitrogen species, cytotoxic adenosine triphosphate, and glutamate.[13,14] These molecules regulate neuronal activity and maintain homeostasis in the brain.[11,15,16] Microglia can be activated in response to various acute stress states where neurons are damaged or repaired.[17] Sugama, *et al*.[18] have shown that restraint stress induces activation of the microglia through the membrane β-adrenergic receptors of the blue spot-norepinephrine system in the brain. Therefore, we hypothesized that the microglia in the CNS play a regulatory role in the central sympathetic nervous system outflow resulting in pathogenetic SCM. The paraventricular hypothalamic nucleus (PVN) is the higher center of the subcortical sympathetic nerves and is also known as the "sympathetic outflow tract", from which sympathetic preganglionic neurons project into the ventral lateral nucleus of the medulla oblongata and descend to the middle ventral lateral column of the spinal cord. These neurons send postganglionic fibers to innervate the neural efferent and cardiac sympathetic afferent reflexes after cervical stellate ganglion permutation.[19] In this study, we investigated the activation of microglia in the PVN of SCM rats and the protective effect of minocycline in inhibiting microglial activation in SCM.

METHODS

Animals and Treatments

Male Sprague-Dawley (SD) rats (300–400 g) were obtained from the Liaoning Changsheng Biotechnology Co., Ltd (Shenyang, China) and randomized into three groups: (1) an SCM model group (n = 23) in which rats were restrained to create immobilization stress (IS), following the methods described in our previous study;[20] (2) a minocycline group (n = 20), which received an intraperitoneal dose of 40 mg/kg of minocycline (M9511-100 MG), and after standing for 2 h, they were subject to the IS experiment, which showed no difference from the model group; and (3) a control group (n = 17), no intervention. All experimental protocols were approved by the Animal Ethics Committee of the First Affiliated Hospital of Harbin Medical University (No.2021096) and adhere to the National Institute Laboratory Guide for the Care and Use of Laboratory Animals.

All of the rats were fed ad libitum and maintained at 21 ± 1 °C under a 12:12 h light:dark cycle. IS commenced at 10:00 am and ended at 4:00 pm, for 7 consecutive days (Figure 1A & 1B). Following the IS trial, surface electrocardiogram (ECG), ultrasonic cardiogram, and intracardiac electrophysiology measurements were recorded after which the rats were anesthetized using 20% urethane (1.5 g/kg) and subjected to tracheal intubation and artificial breathing at 60–80 beats/min, using oxygen-enriched ambient air. After anesthesia, plasma, brain, and left ventricular tissues were collected, rinsed in saline, dried, frozen in liquid nitrogen for 15 min, and then stored at −80 °C.

Surface ECG

We used a multichannel electrophysiological recorder (GY-6000) (Henan Huanan Medical Electric Technology Co., Ltd., Zhengzhou, China) to record the surface ECG of rats for 30 min. The QT interval, QT corrected (QTc) interval, Tpeak-end (Tp-e), and T-wave amplitude were measured for each experimental group. The QTc interval was calculated using Bazett's formula: QT/RR1/2. The Tp-e was defined as the interval from the wave peak to the end of the T-wave. For a more accurate measurement of T-wave duration, we referred to various the previous studies.[21–23]

Ultrasonic Cardiograms

Ultrasonic cardiograms were measured using a Philips EPIQ 5 (Bothell, Washington, USA), and transthoracic echocardiographs were measured using a Philips S12-4 phase-controlled ultrasound transducer (Bothell, Washington, USA). Parasternal short-axis maps we-

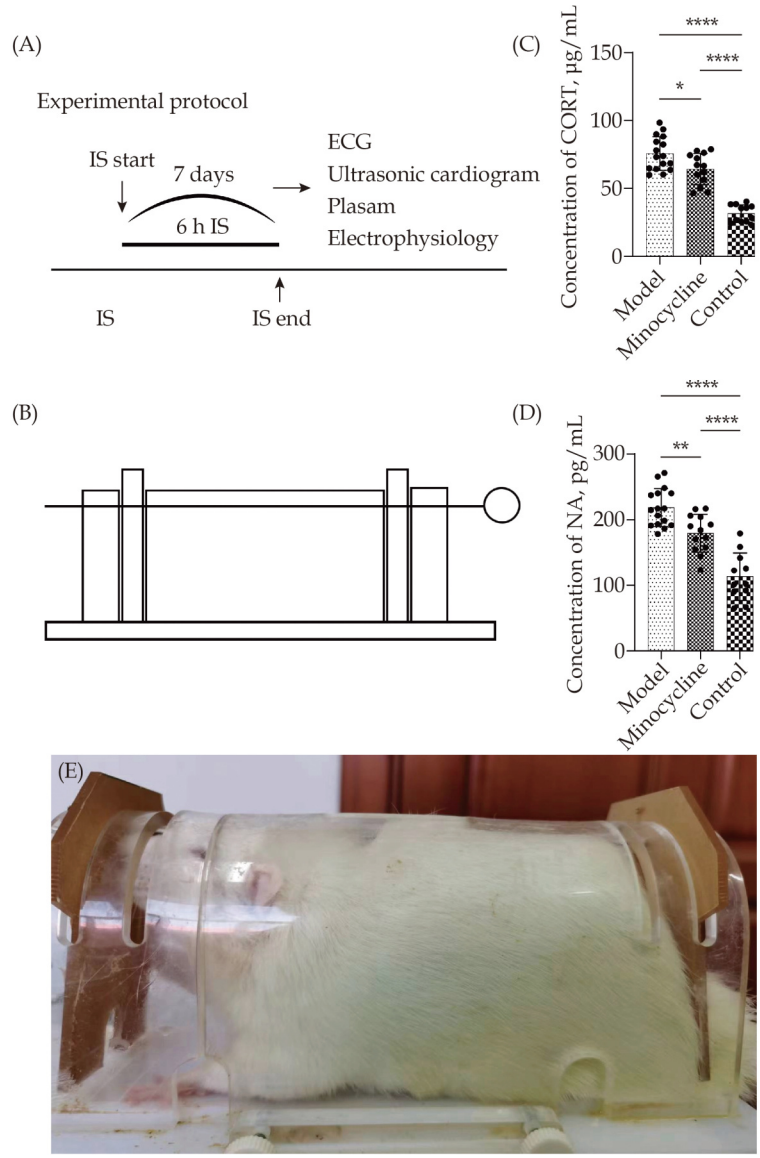

Figure 1 Schematic depiction of the IS protocol. (A): Male Sprague-Dawley rats were subjected to IS for 6 h every day for seven days. Electrocardiogram, ultrasonic cardiogram, plasma, electrophysiology studies were measured following IS; (B): IS device for rats; (C): plasma corticosterone levels in the model, minocycline, and control groups were 75.77 ± 12.43 μg/mL, 64.31 ± 11.54 μg/mL, and 31.53 ± 6.46 μg/mL, respectively; (D): plasma noradrenaline levels in the model, minocycline, and control groups were 218.8 ± 28.88 pg/mL, 179.8 ± 28.82 pg/mL, and 113.3 ± 36.47 pg/mL, respectively; and (E): rat immobilization stress. *P < 0.05, **P < 0.01, ****P < 0.0001. IS: immobilization stress.

re recorded to measure the maximum left ventricular volumes at the end of diastole and systole. The left ventricular ejection fraction (LVEF), left ventricular end-systolic volume (LVESV), and left ventricular end-diastolic volume (LVEDV) were also recorded. The measurements were averaged over three consecutive cardiac cycles, and each echocardiography was performed by the same skilled cardiac sonographer who was unaware of the experimental groupings and the specific experimental protocol.

Cardiac Electrophysiology

Urethane (1.5 g/kg) was injected intraperitoneally to anesthetize the rats. A locust separation along the left parasternal apex was made to expose the heart to allow intracardiac electrophysiology to determine the occurrence of VF and the left ventricular effective refractory period (VERP). A 1.9 F electrophysiological catheter (Transonic Scisense Inc., Ontario, Canada) was placed on the left ventricular apex. Ventricle pacing (20 Hz, 2 ms

pulse width, for 10 s) was used to determine the inducibility of VF. VERP values were determined by delivering a single S2 stimulus after eight times S1. The S1–S1 interval was set at 120 ms. The S1–S2 interval was initially set at 80 ms and then reduced in 2 ms steps until an S2 stimulus could not elicit a ventricular response. The last S1-S2 interval to elicit a ventricular response was defined as the VERP. The ventricular fibrillation threshold (VFT), determined using a train of constant-current pulses (20 Hz, for 10 s), was applied during diastole to induce VF. The voltage was increased from 1 V to 6 V, in 0.5 V (10 s) steps until VF was elicited. The VFT was defined as the lowest voltage required to induce VF. VF was defined as an irregular ventricular arrhythmia lasting for more than 1 s.

Enzyme-linked Immunosorbent Assay (ELISA)

Within 2 h of anesthesia, the intraperitoneal venous blood was collected, placed into ethylenediaminetetraacetic acid tubes, and centrifuged in a cryogenic centrifuge (Beckman, Beverly, CA, USA) at 3000 g for 15 min at 4 °C. The supernatant was then reserved. Plasma samples were stored at −80 °C for later analysis. Noradrenaline (NA), brain natriuretic peptide (BNP), cardiac troponin I (cTnI), and corticosterone (CORT) levels were measured using respective ELISA kits (all from Wuhan Adanti Biotechnology Co., Ltd., Wuhan, China).

Western Blotting

The proteins were separated using electrophoresis on 10% or 12.5% SDS-polyacrylamide gels and transferred to polyvinylidene difluoride membranes while still wet. The membranes were sealed with 5% skimmed dry milk dissolved in phosphate buffer saline and then incubated overnight at 4 °C. The membranes were treated with the primary antibody, incubated overnight, and then exposed to a horseradish peroxidase-coupled secondary antibody for 1 h. Antibodies for markers of microglial activation (anti-IBA-1) (ab178846), central sympathetic nerve activity (c-fos) (ab208942), and peripheral sympathetic expression (Tyrosine hydroxylase, T-H) (ab112) and the inflammatory markers IL-6 (ab9324), IL-1β (ab254360), and TNF-α were purchased from Abcam (Cambridge, UK). GAPDH and β-tubulin were used as internal reference proteins. AlphaView FluorChem FC3 in a Bio-Rad system (Bio-Rad, Hercules, CA, USA) used to view and record the bands.

Immunohistochemistry (IHC)

The brains were collected and fixed in paraformaldehyde solution for 24 h. The PVN area was cut in the coronal plane, divided into sections, rinsed with water for 2 h, dehydrated in an ethanol gradient, and embedded in paraffin. The ethanol gradient dehydration routine followed the protocol, then, 3% hydrogen peroxide was added to the sections for 30 min followed by placement in citrate solution for microwave antigen repair and acclimation to room temperature. Next, the sections were washed with PBST solution (100 mL Phosphate buffer saline + 20 μL Tween) three times for 5 min each time, blocked with goat serum for 30 min, and incubated with primary antibody (anti-IBA1 rabbit antibody, 1:2000, Abcam and anti-c-fos mouse antibody, 1:2000, Abcam) overnight at 4 °C. The sections were washed in PBST three times for 5 min each time, then incubated with horseradish peroxidase-labeled goat anti-rabbit/mouse IgG (anti-rabbit: 1:10000, ZB-5301, ZSGB-BIO, Beijing, China; anti-mouse: 1:10000, ZB-2305, ZSGB-BIO, Beijing, China) for 30 min. DAB was then added dropwise to the sections and allowed to incubate for 3 min, then, hematoxylin re-staining and counterstaining, dehydration, and coverslipping.

Cell Counting and Analysis

The IBA1-immunoreactive (IBA1-IR) microglia in the PVN were counted over a grid with a 100 μm scale and photographed. Each complete microglial nucleus with branches was defined as one microglia. The average of three photographs was taken as the final result of the cell count. The most commonly observed cell morphology in the PVN was chosen and photographed to represent the typical IBA1-IR microglial morphology at a scale of 50 μm.

RNA Sequencing and Data Analysis

Brains from the rats in the control, model, and minocycline groups were collected seven days after IS. Total RNA was isolated using Trizol Reagent (Invitrogen Life Technologies, Waltham, MA, USA), and sequencing libraries were constructed. RNA sequencing was performed using an Illumina HiSeq X Ten (Illumina, San Diego, CA, USA). Raw sequencing data were filtered using the FASTP (v.0.22.0) software to remove connectors and low-quality reads. The filtered data were mapped to the rat reference genome using the HISAT2 (v.2.1.0) soft-

ware, and the gene expression levels were then calculated using the HTSeq (v.0.9.1) software. Differentially expressed genes (DEGs) between groups were identified using the edgeR (v.3.42.4) algorithm in R (v.4.3.1). Genes with a $\log_2$FoldChange ≥ 0.5 or ≤ −0.5 and a $P < 0.05$ were defined as DEGs. Analysis of the DEGs was performed using clusterProfiler[24] (v.4.8.3) to assign Gene Ontology Biological Processes, with a cutoff significance set at $P < 0.05$. The raw RNA sequencing data are available from the National Center for Biotechnology Information Gene Expression Omnibus database under the accession number GSE261833.

Statistical Analysis

Except for VF duration, normally distributed data were reported as mean ± SD. Data from skewed distributions were expressed as the median (interquartile range, 25%–75%). One-way ANOVA analysis (*F*-test) and Bonferroni's test were used to compare normally distributed data between the different experimental groups. The Kruskal-Wallis test combined with pairwise comparisons was used to compare skewed distribution data among the different groups. A two-tailed probability value of $P < 0.05$ was considered statistically significant.

RESULTS

SCM Rats had Higher Concentrations of Stress Hormones

After IS, most of the rats displayed stress symptoms such as upright hair, irritability, and red discharge around the eyes. To evaluate the degree of stress, plasma CORT, and NA levels were measured using ELISA kits (Figure 1C & 1D). Compared with the control group, the plasma CORT levels in the model group increased from 31.53 ± 6.46 μg/mL ($n = 11$, $P < 0.0001$) before IS to 75.77 ± 12.43 μg/mL ($n = 16$, $P < 0.0001$) after IS, while the CORT levels decreased to 64.31 ± 11.54 μg/mL ($n = 13$, $P < 0.05$) after minocycline treatment. Comparing to the control group, the model group plasma NA levels increased from 113.3 ± 36.47 pg/mL ($n = 11$, $P < 0.0001$) to 218.8 ± 28.88 pg/mL ($n = 16$, $P < 0.0001$), and after minocycline treatment, NA levels decreased to 179.8 ± 28.82 pg/mL ($n = 13$, $P < 0.01$) (Figure 1C & 1D). These results showed that the IS protocol effectively induced stress in SD rats, and that minocycline treatment was able to reduce the levels of stress-related hormones.

SCM Rats Exhibited Spontaneous Premature Ventricular Contractions with Altered Ventricular Structure and Function

The ECG analysis revealed significant differences among the three groups in terms of the QT interval, QTc interval, QRS interval, Tp-e, and T-wave amplitude. The QT and T-wave of each lead were quite stable, without abnormal fluctuations. We recorded 30-minute surface ECG values and observed spontaneous ventricular arrhythmias in SCM rats, as shown in Figure 2A, where ventricular premature systolic dyads were recorded in the model group. Compared with the control group, the model group showed obvious differences in the QT interval, QTc interval, Tp-e, and T-wave amplitude. The model group was characterized by prolonged QT and QTc intervals, no difference in QRS interval, increased T-wave amplitude and prolonged Tp-e ($P < 0.05$, Figure 2B–2F). In the minocycline group, the QT interval, QTc interval and Tp-e were clearly improved ($P < 0.0001$, Figure 2B & 2C & 2F).

SCM can be divided into four types: basal Takotsubo syndrome (TTS), midventricular TTS, apical TTS (classical SCM), and focal TTS. Transthoracic parasternal short-axis cardiac M-mode cardiac echocardiography measures were taken to evaluate the effects of the IS protocol on cardiac structure and ventricular motion in the rats (Figure 2G–2I). The results showed that compared with the control group, IS led to a significant decrease in LVEF ($P < 0.0001$), LVESV ($P < 0.0001$), and LVEDV ($P < 0.05$) in the model animals (Figure 2J–2L). In the IS-induced SCM model rats, it seems that impairment of the left ventricular systolic function was more significant than the diastolic function. These findings are similar to those seen in clinical cardiac ultrasound performance in human SCM patients, indicating that the IS-induced SCM model in SD rats could be realistic. Minocycline treatment significantly improved the LVESV and LVEF ($P < 0.05$, $P < 0.0001$, respectively) but had no significant effect on the LVEDV ($P > 0.05$, Figure 2J–2L).

SCM Rats Showed Reduced Myocardial Injury and Ventricular Electrical Stability

Previous studies have demonstrated elevated plasma stress-related hormone levels in SCM rats (Figure 1C & 1D). The rate of VF induction, VERP, and VFT were calculated to determine the electrical stability of the ventricles (Figure 3A–3C & Figure 3F–3H). The levels of

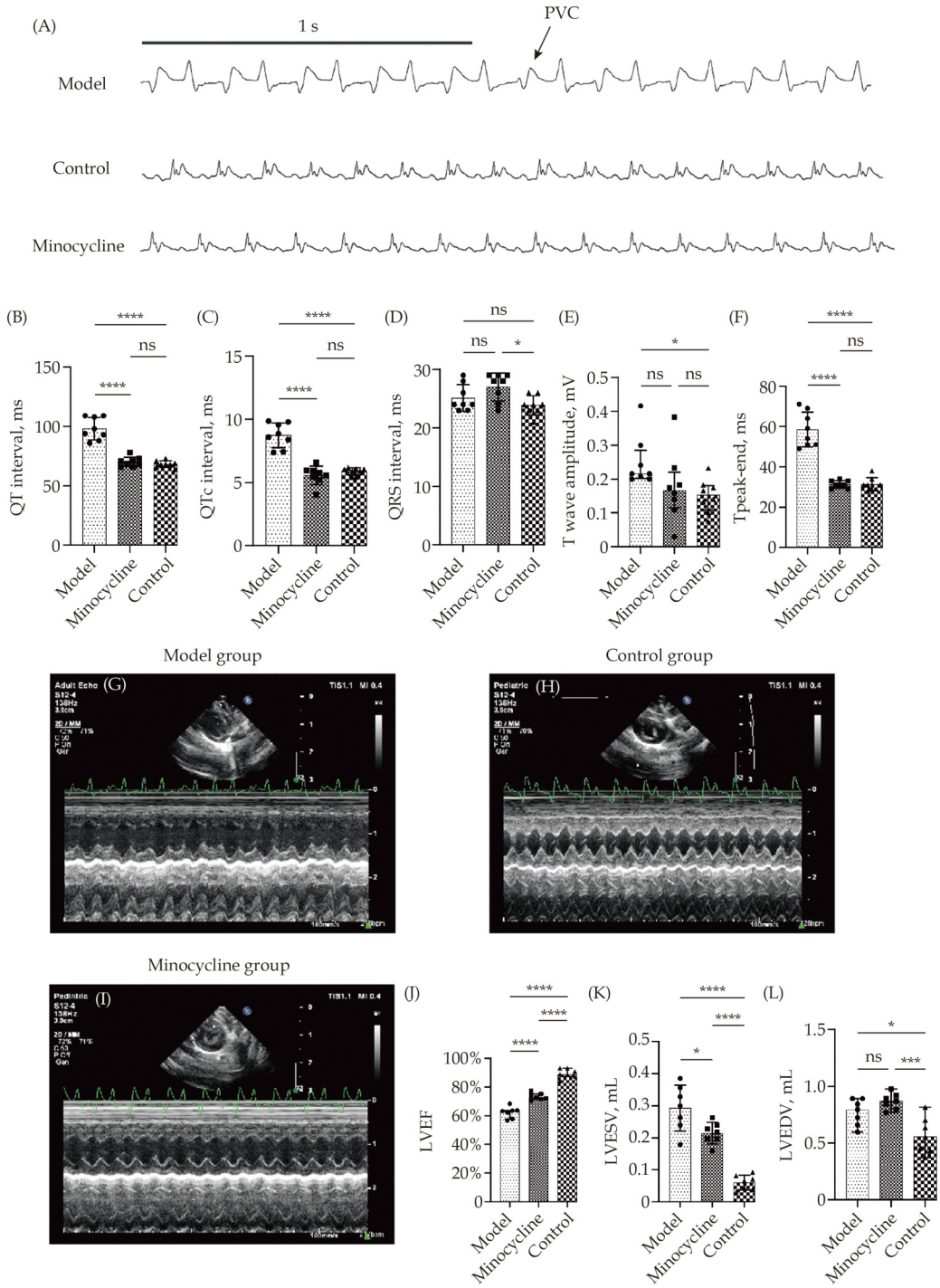

Figure 2 Alterations in ventricular structure, function, and electrical stability. (A): Spontaneous frequent premature ventricular contraction occurred in 11 electrocardiograms in the model group, but not in the minocycline and control groups; (B–F): statistical histograms of the QT interval, QTc interval, QRS interval, T-wave amplitude, and Tp-e in the model, minocycline, and control groups. QT interval: 98.13 ± 9.46 ms, 70.25 ± 3.40 ms, 68.38 ± 2.78 ms; QRS intervals: 25.13 ± 2.30 ms, 27 ± 2.39 ms, 23.88 ± 1.64 ms; Tp-e: 58.5 ± 8.62 ms, 31.38 ± 1.85 ms, 31.38 ± 3.25 ms; and T-wave amplitudes: 0.2160 (0.20-0.2853) mv, 0.1665 (0.1163-0.2205) mv, 0.1535 (0.1083-0.1810) mv, respectively (n = 8 per group); (G–I): each image is a short-axis M-mode ultrasound image at the apical, papillary muscle level site of the left ventricle; and (J–L): histograms of LVEF, LVESV, and LVEDV statistics for the model, control, and minocycline groups. *P < 0.05, ***P < 0.001, ****P < 0.0001, ns for no difference. LVEDV: left ventricular end-diastolic volume; LVEF: left ventricular ejection fraction; LVESV: left ventricular end-systolic volume; QTc: QT corrected; Tp-e: Tpeak-end.

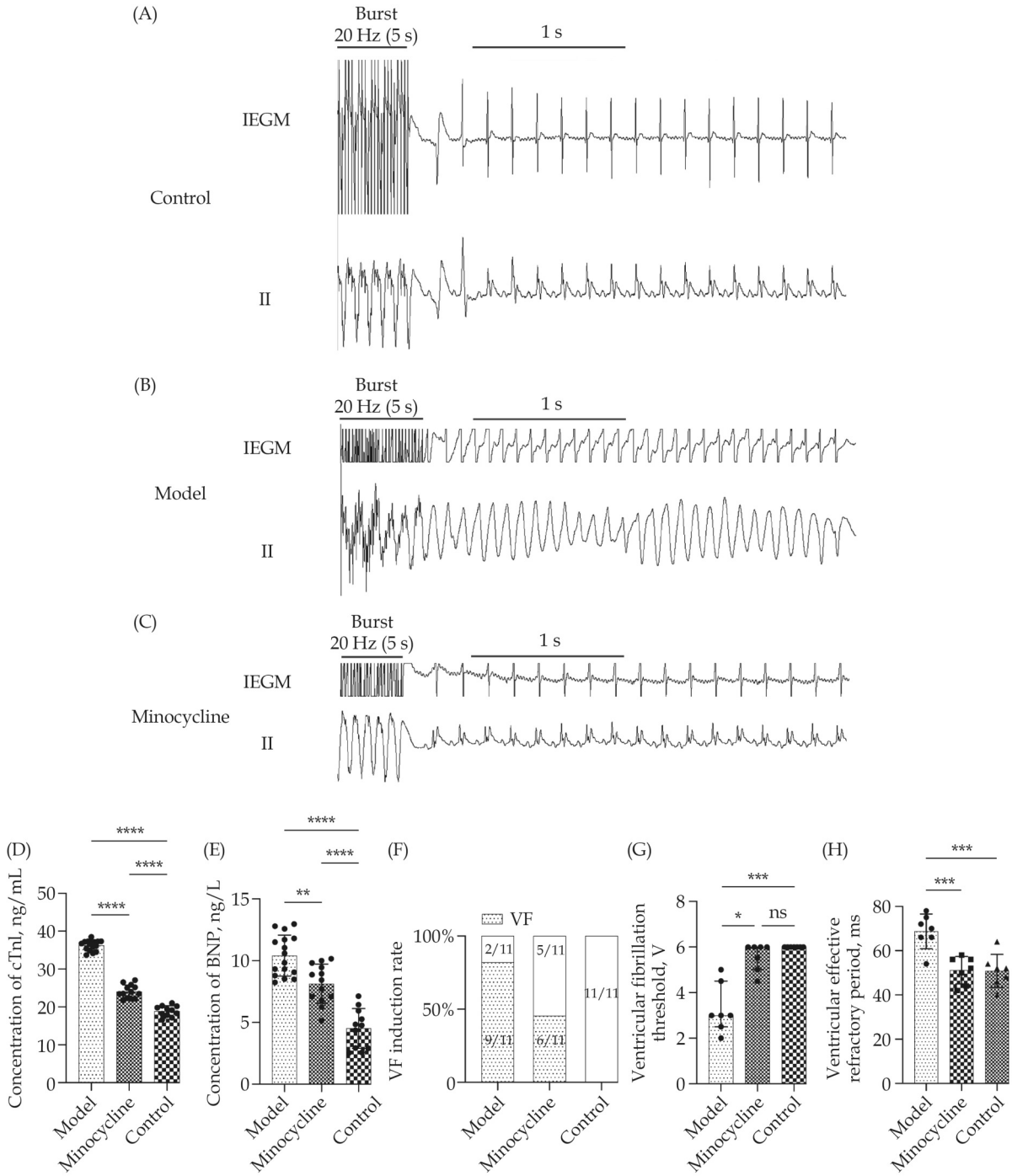

Figure 3 Inhibition of microglial activation improved ventricular electrophysiology and myocardial injury. (A): Induced VF failed in the control group and the sinus rate resumed within 1 s after the stimulation ended (n = 11); (B): VF was successfully induced, and lasted for > 1 min in three rats (n = 11); (C): induced VF failed in the minocycline group (n = 11); (D & E): ELISA statistical histograms of plasma cTnI and BNP concentrations. The cTnI concentrations in the model, minocycline, and control groups were 36.22 ± 1.36 ng/mL, 24.04 ± 1.75 ng/mL, and 18.91 ± 1.39 ng/mL, respectively. The plasma BNP concentrations in the model, minocycline, and control groups were 10.41 ± 1.659 ng/L, 8.137 ± 1.59 ng/L, and 4.516 ± 1.615 ng/L, respectively (model group: n = 16; minocycline group: n = 13; control group: n = 11); (F): the percentage of VF induced rats in each group (n = 11 per group); (G): the ventricular fibrillation threshold in each group (n = 7 per group); and (H): the ventricular effective refractory period in each experimental group (n = 7 per group). *P < 0.05, **P < 0.01, ***P < 0.001, ****P < 0.0001, ns for no difference. BNP: brain natriuretic peptide; cTnI: cardiac troponin I; ELISA: enzyme-linked immunosorbent assay; VF: ventricular fibrillation.

plasma BNP and cTnI were measured to determine the degree of heart injury (Figure 3D & 3E). Figure 3A–3C and Figure 3F shows the VF induction in the model, minocycline, and control groups. We successfully induced VF (VF > 1 s) in the model group using a uniform stimulation procedure, with an induction rate of around 82% (n = 9/11), with about 27% of VF lasting for more than 1 min failing to recover sinus rate. However, VF was not induced in the control group. VF was evoked in some of the minocycline-treated rats, with a 45% induction rate (n = 5/11), and all of the VF rats resumed sinus rate after a sustained period (VF < 1 min). A significant difference in VERP was observed in the model group compared with the control and minocycline groups (P < 0.001) (Figure 3H) (model group: 68.71 ± 2.97 ms; minocycline group: 51.14 ± 2.34 ms; control group: 50.86 ± 2.82 ms). Meanwhile, the VFT of the model group was lower than the other groups [model group: 3.286 ± 1.075 V; minocycline group: 6.0 (5.0-6.0) V; control group: 6.0 (6.0-6.0) V] (Figure 3G). Compared with the control group, the plasma cTnI and BNP levels were significantly higher in the model group (P < 0.0001, Figure 3D & 3E) and those in the minocycline group were significantly lower than those in the model group (P < 0.01, Figure 3D & 3E). These results indicate that minocycline inhibition of microglial activation successfully attenuates stress-related hormone levels and cardiac damage in SCM rats. The inhibition of microglial activation has a protective effect on myocardial injury and ventricular electrical stability.

RNA Sequencing Revealed the Activation of Microglia and Neuroinflammation in SCM Rats

RNA sequencing was performed on five PVN tissues in the model, minocycline, and control groups. The sequencing results are shown in Figure 4A–4C. The DEGs of the model group were compared with the control group, and a volcano plot was generated (|$\log_2$FoldChange| > 0.5 and P < 0.05, Figure 4A). A total of 211 up-regulated genes and 292 down-regulated genes were selected for analysis. All of the upregulated DEGs were screened and it was revealed that *Fgf2* acts as a fibroblast growth factor that enhances microglial migration,[25] *Hmgb2* promotes the inflammatory response of microglia,[26] and the expression of *Hif3α* in inflammatory states may be regulated by microglia through the *NF-κB* pathway.[27] It has been reported that *Apoc1* expression in the CNS is unique to microglia.[28] *Clec7a* is one of the markers for microglia (Figure 4A).[29] The results suggest that the activity of microglia in the PVN may be involved in the central mechanism of SCM by regulating neuroinflammation in the model rats. Therefore, we administered minocycline to inhibit microglial activation and then performed differential gene analysis between the minocycline group and the model group (Figure 4B). The results showed that the expressions of *Hif3α*, *Fgf2*, *Apoc1*, *Rgs1*, and *Btg2* were down-regulated, and that *Rgs1* and *Btg2* appeared to be related to the regulation of microglia.[30] In subsequent experiments, an elevation of IBA1, a marker for microglial activation, was also demonstrated (Figure 5J). Subsequently, we performed GO analysis of the DEGs between the minocycline and model groups, and found significant differences in the biological functions of genes in the "regulation of inflammatory factors", "migration of inflammatory cells", "production and regulation of tumor necrosis factor", "production and regulation of IL-1β", and "production and regulation of IL-6" categories (P < 0.05, Figure 4C). In the following experiment, we selected brain tissue from the PVN and performed western blot analyses of IL-6, IL-1β, and TNF-α. The results were consistent with the transcriptome data, demonstrating that the model group had higher levels of IL-6, IL-1β, and TNF-α compared with the minocycline and control groups (Figure 4D–4I). These results suggest that microglia may be involved in the regulation of the central mechanisms of SCM by regulating neuroinflammation in the SCM rats, and that minocycline can inhibit the activation of microglia and reduce the expression of neuroinflammatory factors, such as IL-6, IL-1β, and TNF-α in the PVN.

Microglial and Central Sympathetic Activation in SCM Rats

After IS, the IBA1-IR cells (microglia) exhibited changes in both quantity and morphology in SCM rats (Figure 5A–5I), with an activated phenotype characterized by more branches and thicker cytosol compared with the minocycline and control groups. Furthermore, we observed an increase in the number of IBA1-IR cells and elongated brown branches in the PVN (Figure 5G–5I). We were surprised to discover that c-fos expression followed a similar trend to the IBA1-IR cells (Figures 5 & 6). The IBA1-IR cell enrichment and high c-fos expression were co-located in the PVN (Figure 6). The results of the western blots and statistical analyses of IBA1 (Figure 5J & 5K) and c-fos (Figure 6G & 6I) were consistent with the IHC results.

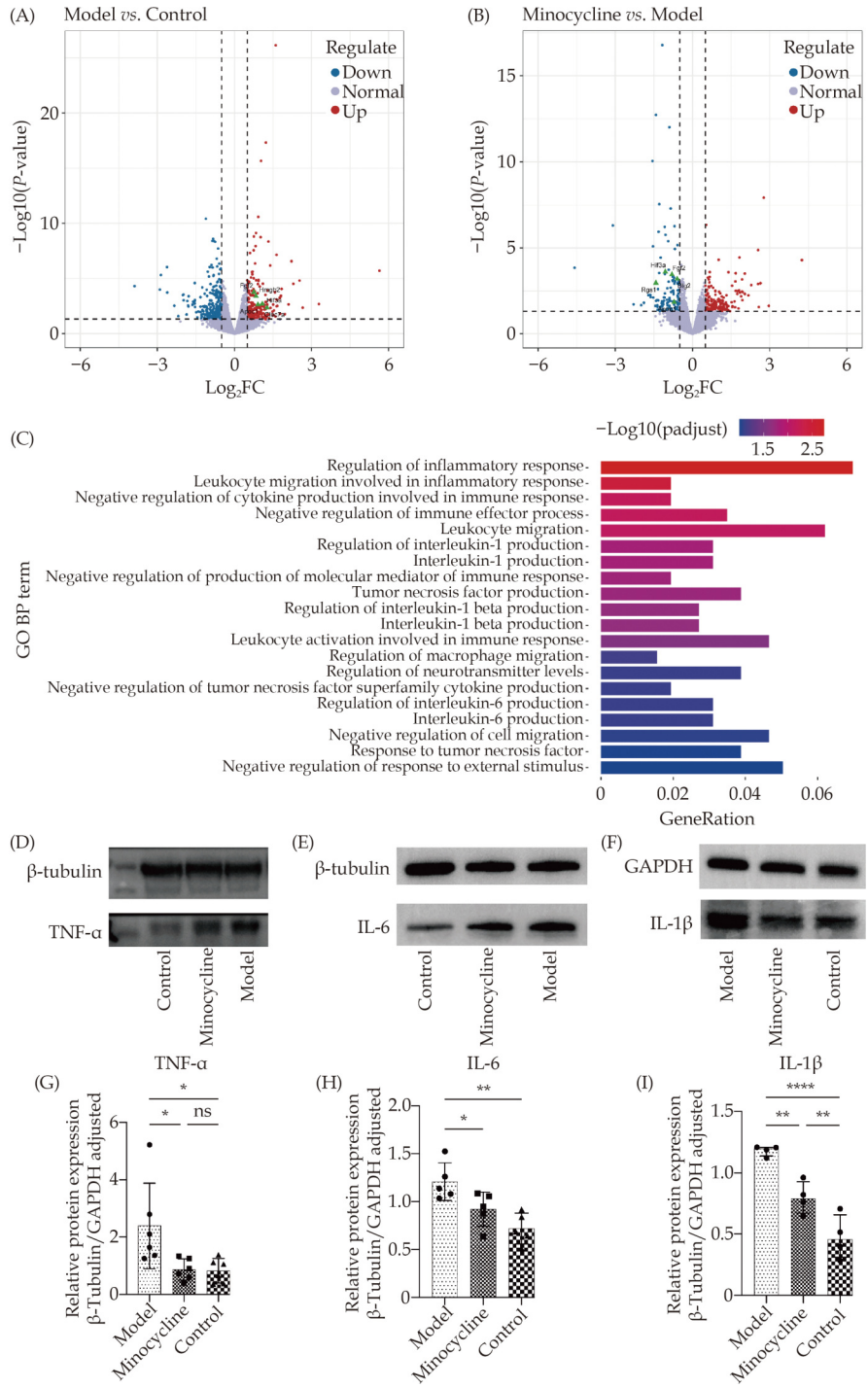

Figure 4 Microglia and neuroinflammation activation are highlighted in SCM. (A): Volcano plot to initially screen the differentially expressed genes between the model and control groups ($P < 0.05$). The labeled genes are *Fgf2, Hmgb2, Hif3α, Apoc1,* and *Clec7a*; (B): volcano plot to initially screen the differentially expressed genes between the minocycline and model groups ($P < 0.05$). The labeled genes are *Hif3a, Fgf2, Btg2, Rgs1,* and *Apoc1*; (C): the enrichment of genes in the GO biological function categories. The range and median *P*-values for the different specific biological functions within each category are shown. The size of the rectangle indicates the number of genes and the shade of the color indicates the corrected *P*-value. The smaller the corrected *P*-value, the closer it is to red; and (D–I): western blotting and statistical analysis of the PVN for TNF-α, IL-6, and IL-1β with GAPDH/β-tubulin as the internal reference protein (TNF-α and IL-6: $n = 5$ per group; IL-1β: $n = 4$ per group). Transcriptomic samples in each group of $n = 5$. *$P < 0.05$, **$P < 0.01$, ****$P < 0.0001$, ns for no difference. PVN: paraventricular hypothalamic nucleus; SCM: stress cardiomyopathy.

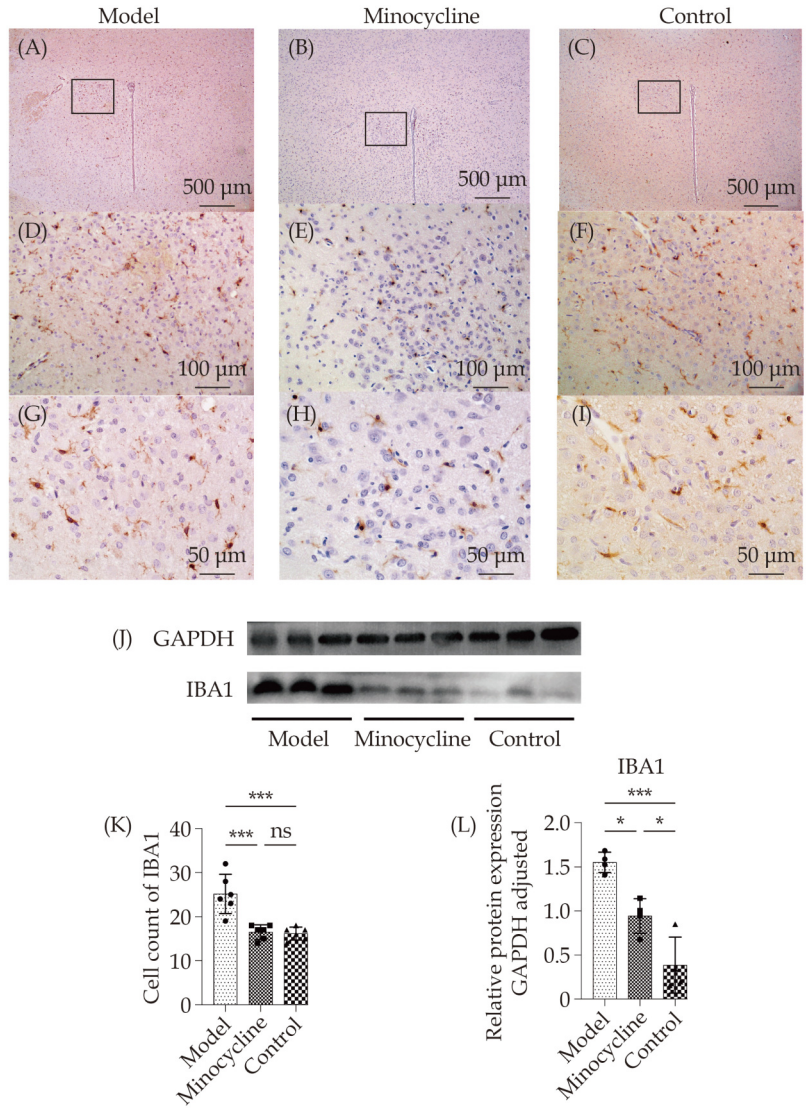

Figure 5 Changes in the microglia in the PVN. (A–C): The location of the PVN is shown in the rectangle. Scale bar: 500 μm; (D–F): the part of the PVN shown in A–C. Scale bar: 100 μm; (G–I): the part of the PVN shown in D–F. Scale bar: 50 μm. Activated IBA1-IR cells in the PVN of stress cardiomyopathy rats (G), the IBA1-IR cells inhibited through minocycline treatment (H) and the "resting" IBA1-IR cells (I); (J): representative western blots of microglia IBA1; (K): histograms showing the cell counts of microglial Iba1-IR (n = 6 per group); and (L): quantification of IBA1 using GAPDH as the internal reference protein (model group: n = 4; minocycline group: n = 4; control group: n = 4). *P < 0.05, ***P < 0.001, ns for no difference. PVN: paraventricular hypothalamic nucleus.

Increased Peripheral Cardiac Sympathetic Ventricular Nerve Activity in SCM Rats

In order to verify whether the peripheral sympathetic activity of the heart was affected by the central sympathetic activity western blots were used to analyze the expression of T-H (a marker of sympathetic synapses) in the left ventricular myocardium. The results are shown in Figure 6H. The expression of T-H was significantly higher in the model group compared with the minocycline and control groups (P < 0.05), while there was no difference between the minocycline and the control groups (P > 0.05; Figure 6J). The results showed that central sympathetic activity influences cardiac sympathetic activity.

DISCUSSION

In this study, we successfully induced an SCM model in SD rats using IS. Previous studies have used drug injection to establish an SCM model, but drug injection modeling has certain limitations, and the drug concentration used often exceeds the physiological upper limit. This

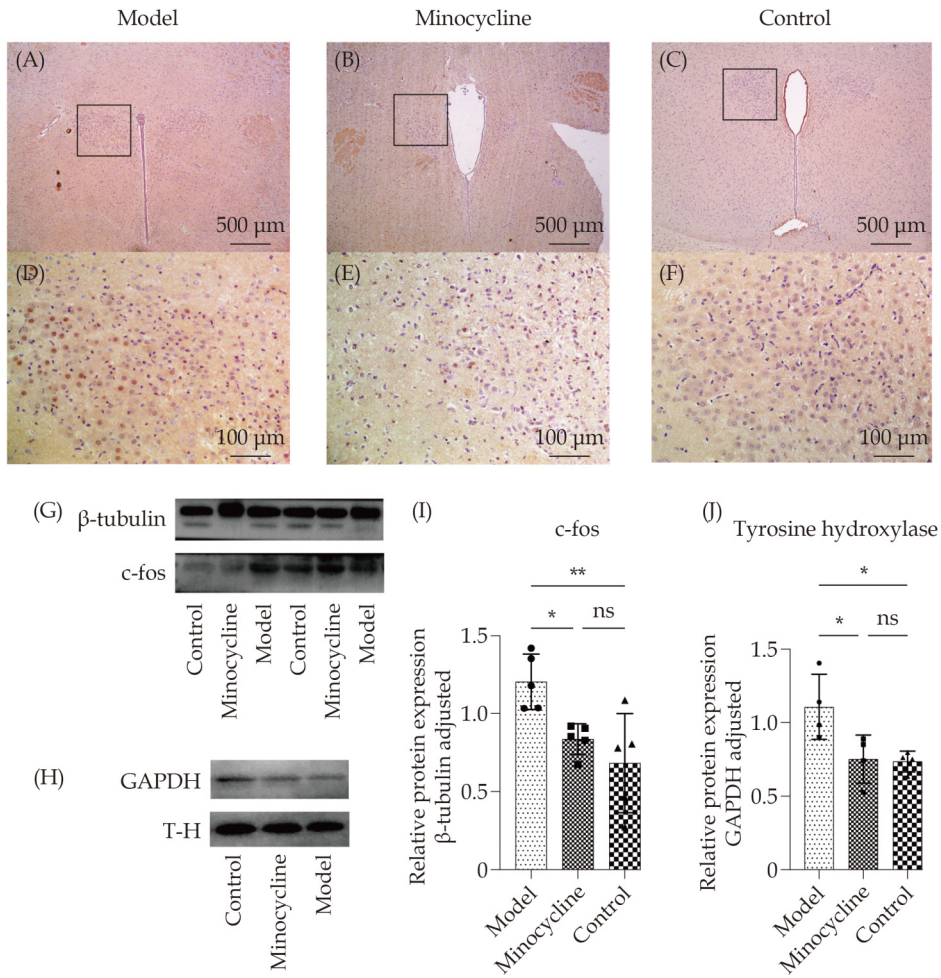

Figure 6 Central and peripheral sympathetic nerve activation. (A–C): The distribution of c-fos in the PVN. Scale bar: 500 μm; (D–F): selected region of the PVN shown in A–C. Scale bar: 500 μm; (G & H): representative western blots of β-tubulin, c-fos, GAPDH, and T-H in the PVN in rats in all of the experimental groups; and (I & J): quantification of c-fos and T-H in rats in all of the experimental groups, with GAPDH or β-tubulin as the internal reference protein (c-fos: model group: $n = 5$; minocycline group: $n = 5$; control group: $n = 5$. T-H: model group: $n = 4$; minocycline group: $n = 4$; control group: $n = 4$). *$P < 0.05$, **$P < 0.01$, ns for no difference. PVN: paraventricular hypothalamic nucleus.

method does not truly reflect the physiological situation under real stress, and the experimental animals modeled by drug injection often suffer considerable mortality. Therefore, we chose IS to induce the establishment of a rat SCM model, more suitable for imitating the incidence of SCM in human patients.[31–33]

PVN transcriptomics revealed that the microglial marker genes related to microglial regulation were upregulated in SCM rats. Subsequently, minocycline was administered to inhibit the activation of microglia, and it was found that the genes related to IL-1β, IL-6, and TNF-α regulation were altered in the minocycline group. Western blotting results also showed that the IL-1β, IL-6, and TNF-α decreased significantly in the minocycline group. Our results suggest that the SCM rats may experience microglial activation and increased neuron-inflammatory factor expression. As a CNS macrophage, microglia are responsible for secreting and regulating the expression of inflammatory factors, as has been confirmed by many previous studies.[12,34,35] Lopez-Rodriguez, *et al.*[36] have shown that activated microglia cells can release IL-1β in response to lipopolysaccharide stimulation. Also, Jeong, *et al.*[37] have claimed activated microglia can produce proinflammatory factors such as IL-6, IL-1β, and TNF-α after SARS-CoV-2 infection in humans. According to the above research results, the regulation of proinflammatory cytokines secretion by microglia has been very clear, so we will not verify it again.

Our experiments verified the activity of the central and peripheral sympathetic nerves using IHC and western blotting, and found that the activity of the central and peripheral sympathetic nerves increased in IS-induced SCM rats. We speculate that the activation of microglia in SCM rats may increase the expression of inflammatory factors in the CNS, increase the outflow of the central sympathetic nerves, and then increase the sympathetic nerve activity in the peripheral heart, ultimately affecting the function and electrical stability of the ventricle. Kabata, *et al.*[38] have shown a correlation between inflammatory factors and neurons, which can enhance the excitability of neurons under different physiological and pathophysiological conditions. This is consistent with our finding that the expression of inflammatory factors and of c-fos, a marker of central sympathetic nerve activity, are increased in the PVN of SCM rats.

We found some changes in the microglia that differed from those previously reported. In the PVN, the microglial cytosol thickened and branches became thin and long and numerous, in contrast to previous reports of reactive microglia with thickened cytosol and fewer branches.[39–43] We found more microglial branches in the background of IHC stains of the PVN. It seems that microglia form a "synaptic network" or "information network". Therefore, we speculate that these longer branches enhance information transmission between cells. However, due to the limitations of our experiments, we were not able to fully explore and verify this hypothesis. Our experiment provides a reference for the further study of the central nervous mechanism of SCM and adds to the transcriptomic database of the PVN in SCM, providing a transcriptomic reference database for future studies.

LIMITATIONS

There are some shortcomings to our experiment that must be noted. Firstly, the validation of peripheral cardiac sympathetic activity is still weak. Secondly, the ECG data revealed unexpected differences in the QRS intervals between the minocycline and the control groups, which remain to be explained. Last but not least, we found a difference in the T-wave amplitude between the model and minocycline groups, but unfortunately it was not statistically significant. Perhaps this is due to an insufficient sample size, producing inconsistent results. Future studies should seek to solve these limitations and further elucidate the role of microglia in SCM.

CONCLUSIONS

The main finding of this study is that the microglia are significantly activated in the PVN of SD rats in SCM, increasing the number of microglial cells and branches. Activated microglia increase central sympathetic nerve activity outflow by enhancing the expression of inflammatory factors, which then increases VF susceptibility. Inhibition of microglial activation may be able to reduce central inflammation and increase cardiac electrical stability. Therefore, the microglia may be a potential target for intervention in the prevention of sudden death in SCM sufferers.

ACKNOWLEDGMENTS

This study was supported by the National Natural Science Foundation of China (No.82270320), the Postdoctoral Scientific Research Developmental Found (LBH-Q21155), the Distinguished Young Foundations of the First Affiliated Hospital of Harbin Medical University (HYD2020JQ002), and the Science Foundation of the First Affiliated Hospital of Harbin Medical University (No.2018 L001). All authors had no conflicts of interest to disclose. The authors thank Institute of Cardiology, the First Clinical College of Harbin Medical University, Harbin, China for their support in providing experimental venues. Transcriptomics test services were provided by Harbin Botai Bio-Tech Co., Ltd., Harbin, China.

REFERENCES

[1] Szardien S, Möllmann H, Elsässer A, *et al.* [Historical and current pathophysiological concepts of stress (Tako-Tsubo) cardiomyopathy]. *Herz* 2010; 35: 258-264. [In German].
[2] Amin HZ, Amin LZ, Pradipta A. Takotsubo cardiomyopathy: a brief review. *J Med Life* 2020; 13: 3–7.
[3] Medina de Chazal H, Del Buono MG, Keyser-Marcus L, *et al.* Stress cardiomyopathy diagnosis and treatment: JACC State-of-the-Art Review. *J Am Coll Cardiol* 2018; 72: 1955–1971.
[4] Jin X, Ji X, Yin H, *et al.* Identification of potential targets of stress cardiomyopathy by a machine learning algorithm. *CVIA*. Published Online First: 28 February 2024. DOI: 10.15212/CVIA.2024.0011.
[5] Gianni M, Dentali F, Grandi AM, *et al.* Apical ballooning syndrome or takotsubo cardiomyopathy: a systematic review. *Eur Heart J* 2006; 27: 1523–1529.
[6] Gupta S, Gupta MM. Takotsubo syndrome. *Indian Heart J* 2018; 70: 165–174.

[7] Chong TK, Chen J, Lyu L, *et al*. Clinical characteristics and outcome correlates of Chinese patients with takotsubo syndrome: results from the first Chinese Takotsubo Syndrome Registry. *Int J Cardiol* 2023; 387: 131129.
[8] Pena Escobar JA, Aung M, Amin S, *et al*. Pathogenesis of ventricular arrhythmias and its effect on long-term prognosis in patients with takotsubo cardiomyopathy. *Cureus* 2020; 12: e11171.
[9] Pei Q, Mbabazi N, Zou L, *et al*. Mechanisms of myocardial stunning in stress-induced cardiomyopathy. *CVIA*. Published Online First: 10 June 2022. DOI: 10.15212/CVIA.2022.0010.
[10] Nef HM, Möllmann H, Akashi YJ, *et al*. Mechanisms of stress (Takotsubo) cardiomyopathy. *Nat Rev Cardiol* 2010; 7: 187–193.
[11] Pósfai B, Cserép C, Orsolits B, *et al*. New insights into microglia-neuron interactions: a neuron's perspective. *Neuroscience* 2019; 405: 103–117.
[12] Illes P, Rubini P, Ulrich H, *et al*. Regulation of microglial functions by purinergic mechanisms in the healthy and diseased CNS. *Cells* 2020; 9: 1108.
[13] Ransohoff RM, Perry VH. Microglial physiology: unique stimuli, specialized responses. *Annu Rev Immunol* 2009; 27: 119–145.
[14] Smith JA, Das A, Ray SK, *et al*. Role of pro-inflammatory cytokines released from microglia in neurodegenerative diseases. *Brain Res Bull* 2012; 87: 10–20.
[15] Marinelli S, Basilico B, Marrone MC, *et al*. Microglia-neuron crosstalk: signaling mechanism and control of synaptic transmission. *Semin Cell Dev Biol* 2019; 94: 138–151.
[16] Liu Y, Li M, Zhang Z, *et al*. Role of microglia-neuron interactions in diabetic encephalopathy. *Ageing Res Rev* 2018; 42: 28–39.
[17] Zhao SC, Ma LS, Chu ZH, *et al*. Regulation of microglial activation in stroke. *Acta Pharmacol Sin* 2017; 38: 445–458.
[18] Sugama S, Takenouchi T, Hashimoto M, *et al*. Stress-induced microglial activation occurs through β-adrenergic receptor: noradrenaline as a key neurotransmitter in microglial activation. *J Neuroinflammation* 2019; 16: 266.
[19] Jiang Z, Rajamanickam S, Justice NJ. CRF signaling between neurons in the paraventricular nucleus of the hypothalamus (PVN) coordinates stress responses. *Neurobiol Stress* 2019; 11: 100192.
[20] Pei Q, Yang J, Li B, *et al*. Histological and functional assessment of a Takotsubo cardiomyopathy model established by immobilization stress. *Pacing Clin Electrophysiol* 2024; 47: 373–382.
[21] Izumi D, Chinushi M, Iijima K, *et al*. The peak-to-end of the T wave in the limb ECG leads reflects total spatial rather than transmural dispersion of ventricular repolarization in an anthopleurin: a model of prolonged QT interval. *Heart Rhythm* 2012; 9: 796–803.
[22] Ye T, Zhang C, Wu G, *et al*. Pinocembrin decreases ventricular fibrillation susceptibility in a rat model of depression. *Front Pharmacol* 2020; 11: 547966.
[23] Oknińska M, Paterek A, Bierła J, *et al*. Effect of age and sex on the incidence of ventricular arrhythmia in a rat model of acute ischemia. *Biomed Pharmacother* 2021; 142: 111983.
[24] Wu T, Hu E, Xu S, *et al*. clusterProfiler 4. *0: a universal enrichment tool for interpreting omics data. Innovation (Camb)* 2021; 2: 100141.
[25] Noda M, Takii K, Parajuli B, *et al*. FGF-2 released from degenerating neurons exerts microglial-induced neuroprotection via FGFR3-ERK signaling pathway. *J Neuroinflammation* 2014; 11: 76.
[26] Yang P, He J, Wang C, *et al*. Downregulation of high mobility group box 2 relieves spinal cord injury by inhibiting microglia-mediated neuroinflammation. *Exp Anim* 2023; 72: 199–208.
[27] Kumar H, Lim JH, Kim IS, *et al*. Differential regulation of HIF-3α in LPS-induced BV-2 microglial cells: comparison and characterization with HIF-1α. *Brain Res* 2015; 1610: 33–41.
[28] Thiel WA, Esposito EJ, Findley AP, *et al*. Modulation of retinoid-X-receptors differentially regulates expression of apolipoprotein genes apoc1 and apoeb by zebrafish microglia. *Biol Open* 2022; 11: bio058990.
[29] Lee J, Kim DE, Griffin P, *et al*. Inhibition of REV-ERBs stimulates microglial amyloid-beta clearance and reduces amyloid plaque deposition in the 5XFAD mouse model of Alzheimer's disease. *Aging Cell* 2020; 19: e13078.
[30] McGill MM, Richman AR, Boyd JR, *et al*. p38 MAP kinase signaling in microglia plays a sex-specific protective role in CNS autoimmunity and regulates microglial transcriptional states. *Front Immunol* 2021; 12: 715311.
[31] Godsman N, Kohlhaas M, Nickel A, *et al*. Metabolic alterations in a rat model of takotsubo syndrome. *Cardiovasc Res* 2022; 118: 1932–1946.
[32] Angelini P, Gamero MT. What can we learn from animal models of Takotsubo syndrome? *Int J Cardiol* 2019; 281: 105-106.
[33] Yoganathan T, Perez-Liva M, Balvay D, *et al*. Acute stress induces long-term metabolic, functional, and structural remodeling of the heart. *Nat Commun* 2023; 14: 3835.
[34] Pahan P, Xie JY. Microglial inflammation modulates opioid analgesic tolerance. *J Neurosci Res* 2023; 101: 1383–1392.
[35] Calcia MA, Bonsall DR, Bloomfield PS, *et al*. Stress and neuroinflammation: a systematic review of the effects of stress on microglia and the implications for mental illness. *Psychopharmacology (Berl)* 2016; 233: 1637–1650.
[36] Lopez-Rodriguez AB, Hennessy E, Murray CL, *et al*. Acute systemic inflammation exacerbates neuroinflammation in Alzheimer's disease: IL-1β drives amplified responses in primed astrocytes and neuronal network dysfunction. *Alzheimers Dement* 2021; 17: 1735–1755.
[37] Jeong GU, Lyu J, Kim KD, *et al*. SARS-CoV-2 infection of microglia elicits proinflammatory activation and apoptotic cell death. *Microbiol Spectr* 2022; 10: e0109122.
[38] Kabata H, Artis D. Neuro-immune crosstalk and allergic inflammation. *J Clin Invest* 2019; 129: 1475–1482.
[39] Laming PR, Kimelberg H, Robinson S, *et al*. Neuronal-glial interactions and behaviour. *Neurosci Biobehav Rev* 2000; 24: 295–340.
[40] Wang Y, Yin J, Wang C, *et al*. Microglial Mincle receptor in the PVN contributes to sympathetic hyperactivity in acute myocardial infarction rat. *J Cell Mol Med* 2019; 23: 112–125.
[41] Lan X, Han X, Li Q, *et al*. Modulators of microglial activa-

tion and polarization after intracerebral haemorrhage. *Nat Rev Neurol* 2017; 13: 420–433.

[42] Bassett B, Subramaniyam S, Fan Y, *et al*. Minocycline alleviates depression-like symptoms by rescuing decrease in neurogenesis in dorsal hippocampus via blocking microglia activation/phagocytosis. *Brain Behav Immun* 2021; 91: 519–530.

[43] Walker FR, Nilsson M, Jones K. Acute and chronic stress-induced disturbances of microglial plasticity, phenotype and function. *Curr Drug Targets* 2013; 14: 1262–1276.

Please cite this article as: LIN PQ, PEI QW, LI B, YANG JM, ZOU LN, SU DZ, ZHANG JP, YIN HP, Nadine M, YANG JJ, A NV, Musawir Abbas K, JIANG ZL, LI JJ, YIN DC. The effects of hypothalamic microglial activation on ventricular arrhythmias in stress cardiomyopathy. *J Geriatr Cardiol* 2024; 21(12): 1119–1132. DOI: 10.26599/1671-5411.2024.12.002